Geometric Snakes for Edge Detection and Segmentation of Medical Imagery

Anthony Yezzi, Jr.
Department of Electrical Engineering
University of Minnesota
Minneapolis, MN 55455
email: ayezzi@ee.umn.edu

Arun Kumar
Department of Aerospace Eng.
University of Minnesota
Minneapolis, MN 55455
email: arun@aem.umn.edu

Satyanad Kichenassamy
Department of Mathematics
University of Minnesota
Minneapolis, MN 55455
email: kichenas@math.umn.edu

Peter Olver
Department of Mathematics
University of Minnesota
Minneapolis, MN 55455
email: olver@ima.umn.edu

Allen Tannenbaum *
Department of Electrical Engineering
University of Minnesota
Minneapolis, MN 55455
email: tannenba@ee.umn.edu

This work was supported in part by grants from the National Science Foundation DMS-9204192 and ECS-9122106, by the Air Force Office of Scientific Research F49620-94-1-0058DEF, by the Army Research Office DAAH04-94-G-0054 and DAAH04-93-G-0332, and by Image Evolutions Limited.

This paper has been submitted to the **IEEE Transaction of Medical Imaging**

*Please send all correspondence to this author.

Abstract

In this paper, we employ the new geometric active contour models formulated in [20, 21] for edge detection and segmentation of MRI and ultrasound medical imagery. Our method is based on defining feature-based metrics on a given image which in turn leads to a novel snake paradigm in which the feature of interest may be considered to lie at the bottom of a potential well. Thus the snake is attracted very naturally and efficiently to the desired feature.

Key words: Active vision, active contours, snakes, edge detection, segmentation, gradient flows.

1 Introduction

The technique of *snakes* or *active contours* has become quite popular for a variety of applications in the past few years. This methodology is based upon the utilization of deformable contours which conform to various object shapes and motions. Snakes have been used for edge and curve detection, segmentation, shape modelling, and visual tracking. The technique has also been widely applied for various applications in medical imaging. For example, snakes have been employed for the segmentation of myocardial heart boundaries as a prerequisite from which such vital information such as ejection-fraction ratio, heart output, and ventricular volume ratio can be computed. See [17, 35] and the references therein. In this paper, we will apply a new snake paradigm which the authors have developed in [20, 21] for edge detection and segmentation of various kinds of medical imagery including MRI and ultrasound.

In the classical theory of snakes, one considers energy minimization methods where controlled continuity splines are allowed to move under the influence of external image dependent forces, internal forces, and certain contraints set by the user. See [19, 44, 6]. As is well-known there may be a number of problems associated with this approach such as initializations, existence of multiple minima, and the selection of the elasticity parameters.

In this work, we will apply a new active contour method which was developed in [20, 21]. Our approach employs ideas from Euclidean curve shortening evolution which defines the gradient direction in which the Euclidean perimeter is shrinking as fast as possible. (See Section 3.) We therefore note that we can derive new active contour models by multiplying the Euclidean arc-length by a function tailored to the features of interest to which we want to flow, and then writing down the resulting *gradient evolution equations.* Mathematically, this amounts to defining a new Riemannian metric in the plane tailored to the given image, and then computing the corresponding gradient flow. This leads to some new snake models which efficiently attract the given active contour to the features of interest (which basically lie at the bottom of a *potential well*). The method also allows us to naturally write down 3-D active surface models for three dimensional image segmentation as well which we do in [20, 21]. One can completely justify this method using viscosity theory which is done as well in [20, 21].

The contents of this paper may be summarized as follows. In Section 2, we briefly sketch some background from the classical theory of snakes. In Section 3, we give the relevant from curve evolution theory, which allows us to formulate our new active contour paradigm in Section 4. In Section 5, we indicate how these methods may be extended for volumetric segmentation based on mean curvature flow. Finally in Section 6, we apply our methods to some specific medical images, and then we draw our conclusions in Section 7.

2 Background on Snakes

In this section, we briefly review the energy based optimization approach to deformable contours as discussed in [19, 44, 10, 6]. For complete details, we refer the interested reader to the collection of papers in [6], especially [43].

Let $C(p) = (x(p), y(p))^T$ be a closed contour in R^2 where $0 \leq p \leq 1$. (Note that the superscript T denotes transpose.) We now define an energy functional on the set of such contours ("snakes"), $\mathcal{E}(C)$. Following standard practice, we take $\mathcal{E}(C)$ to be of the form

$$\mathcal{E}(C) = \mathcal{E}_{int}(C) + \mathcal{P}(C),$$

where $\mathcal{E}_{int}$ is the *internal deformation energy* and $\mathcal{P}$ is an external potential energy which depends on the image. (Other external constraint forces may be added.) Perhaps the most common choice for the internal energy is the quadratic functional

$$\mathcal{E}_{int}(C) := \int_0^1 w_1(p)\|C_p\|^2 + w_2(p)\|C_{pp}\|^2 dp,$$

where w_1 and w_2 control the "tension" and "rigidity" of the snake, respectively. (Note that the subscripts denote derivatives with respect to p in the latter expression, and $\|\cdot\|$ denotes the standard Euclidean norm.)

Let $I : R^2 \to R$ be the given grey-scale image. Then the external potential energy depends on the image $I(x, y)$. It can be defined by

$$\mathcal{P}(C) := \int_0^1 P(C(p))dp,$$

where $P(x, y)$ is a scalar potential function defined on the image plane. The local minima of P attract the snake. For example, we may choose P to be

$$P(x, y) := c\|\nabla G_\sigma * I(x, y)\|,$$

for a suitably chosen constant c, in which case the snake will be attracted to intensity edges. Here G_σ denotes a Gaussian smoothing filter of standard deviation σ.

One also typically considers dynamic time-varying models in which $C(p)$ becomes a function of time as well; see [43]. In this case, one defines a kinetic energy and the corresponding Lagrangian (the difference between the kinetic energy and the energy $\mathcal{E}$ defined above). Applying the principle of least action, one derives the corresponding Lagrange equation which one tries to solve numerically employing various approximations.

In the approach to be given below in Section 4, we will also use an energy method. However, in contrast to more *ad hoc* approaches, we believe that our energy is intrinsic to the given geometry of the problem, as is the correspondent gradient flow.

3 Curve Shortening

The mathematical foundation of our new active contour model is based on *Euclidean curve shortening.* Consequently, we will now review the relevant curve evolution theory in the plane R^2.

Accordingly, for κ the curvature, and $\vec{\mathcal{N}}$ the inward unit normal, one considers families of plane curves evolving according to the *geometric heat equation*

$$\frac{\partial C}{\partial t} = \kappa \vec{\mathcal{N}}. \tag{1}$$

This equation has a number of properties which make it very useful in image processing, and in particular, the basis of a nonlinear scale-space for shape representation [1, 3, 22, 23].

In particular, (1) is the Euclidean curve shortening flow, in the sense that the Euclidean perimeter shrinks as quickly as possible when the curve evolves according to (1) [14, 16]. Since, we will need a similar argument for the snake model we discuss in the next section, let us work out the details.

Let $C = C(p,t)$ be a smooth family of closed curves where t parametrizes the family and p the given curve, say $0 \leq p \leq 1$. (Note we assume that $C(0,t) = C(1,t)$ and similarly for the first derivatives.) Consider the length functional

$$L(t) := \int_0^1 \|\frac{\partial C}{\partial p}\| dp.$$

Then differentiating (taking the "first variation"), and using integration by parts, we see that

$$\begin{aligned} L'(t) &= \int_0^1 \frac{\langle \frac{\partial C}{\partial p}, \frac{\partial^2 C}{\partial p \partial t} \rangle}{\|\frac{\partial C}{\partial p}\|} dp \\ &= -\int_0^1 \langle \frac{\partial C}{\partial t}, \frac{1}{\|\frac{\partial C}{\partial p}\|} \frac{\partial}{\partial p} \left[\frac{\frac{\partial C}{\partial p}}{\|\frac{\partial C}{\partial p}\|} \right] \|\frac{\partial C}{\partial p}\| \rangle dp. \end{aligned}$$

(Note that we multiplied and divided by $\|\frac{\partial C}{\partial p}\|$ in the latter integral.) But observing now that

$$\|\frac{\partial C}{\partial p}\| dp =: ds$$

is (Euclidean) arc-length, and using the definition of curvature, the last integral is

$$-\int_0^{L(t)} \langle \frac{\partial C}{\partial t}, \kappa \vec{\mathcal{N}} \rangle ds$$

that is, we see

$$L'(t) = -\int_0^{L(t)} \langle \frac{\partial C}{\partial t}, \kappa \vec{\mathcal{N}} \rangle ds.$$

Thus the direction in which $L(t)$ is decreasing most rapidly is when

$$\frac{\partial C}{\partial t} = \kappa \vec{\mathcal{N}}.$$

Thus (1) is precisely a gradient flow.

A much deeper fact is that simple closed curves converge to "round" points when evolving according to (1) without developing singularities; see [14, 16]. This fact is one of the keys for the geometric active contour models considered below.

4 New Active Contour Paradigm

In some elegant work, Caselles *et al.* [7] and Malladi *et al.* [27] formulate snake models based on the level set formulation of the Euclidean curve shortening equation. Indeed, their model is

$$\frac{\partial \Psi}{\partial t} = \phi(x,y)\|\nabla \Psi\|(\text{div}\left(\frac{\nabla \Psi}{\|\nabla \Psi\|}\right) + \nu). \tag{2}$$

Here the function $\phi(x,y)$ depends on the given image and is used as a "stopping term." For example, the term $\phi(x,y)$ may chosen to be small near an edge, and so acts to stop the evolution when the contour gets close to an edge. In [7, 27], the term

$$\phi := \frac{1}{1 + \|\nabla G_\sigma * I\|^n} \tag{3}$$

is chosen, where I is the (grey-scale) image and G_σ is a Gaussian (smoothing) filter. (In [7], $n = 1$, and in [27], $n = 2$.) The function $\Psi(x,y,t)$ evolves in (2) according to the associated level set flow for planar curve evolution in the normal direction with speed a function of curvature which was introduced in the fundamental work of Osher-Sethian [30, 31, 37, 38, 39].

As we have just seen, the Euclidean curve shortening part of this evolution, namely

$$\frac{\partial \Psi}{\partial t} = \|\nabla \Psi\|\text{div}\left(\frac{\nabla \Psi}{\|\nabla \Psi\|}\right) \tag{4}$$

may be derived as a gradient flow for shrinking the perimeter as quickly as possible using only local information. As is explained in [7], the constant *inflation term* ν is added in (2) in order to keep the evolution moving in the proper direction. Note that we are taking Ψ to be negative in the interior and positive in the exterior of the zero level set contour.

Remarks 1.

1. In [27], the inflationary constant is considered both with a positive sign (inward evolution of the evolution of the contour in the direction of decreasing Ψ) and with a negative sign (outward or expanding evolution). (Note the sign convention we have taken for Ψ above.) In the latter case, this can be referred to as expanding "balloons" or "bubbles" [10, 42].

2. Instead of using a Gaussian to smooth the image one may of course use the a nonlinear smoothing filter based on the curvature; see [4].

3. There are of course many possibilities for a stopping term besides intensity: texture, optical flow, stereo disparity, etc.

We would like to modify the model (2) in a manner suggested by the computation in Section 3. We accomplish this, by changing the ordinary Euclidean arc-length function along a curve $C = (x(p), y(p))^T$ with parameter p given by

$$ds = \|C_p\|dp = (x_p^2 + y_p^2)^{1/2}dp$$

to

$$ds_\phi = \phi ds = (x_p^2 + y_p^2)^{1/2}\phi dp,$$

where $\phi(x, y)$ is a positive differentiable function. We now essentially repeat the computation made in Section 3, i.e., we want to compute the corresponding gradient flow for shortening length relative to the new metric ds_ϕ.

Accordingly set

$$L_\phi(t) := \int_0^1 \|\frac{\partial C}{\partial p}\|\phi dp.$$

Let

$$\vec{\mathcal{T}} := \frac{\partial C}{\partial p}/\|\frac{\partial C}{\partial p}\|,$$

denote the unit tangent. Then taking the first variation of the modified length function L_ϕ, and using integration by parts just as above, we get that

$$-L'_\phi(t) \;=\; \int_0^{L_\phi(t)} \langle \frac{\partial C}{\partial t}, \phi\kappa\vec{\mathcal{N}} + (\nabla\phi \cdot \vec{\mathcal{T}})\vec{\mathcal{T}} - \nabla\phi\rangle ds$$

which means that the direction in which the L_ϕ perimeter is shrinking as fast as possible is given by

$$\frac{\partial C}{\partial t} = \phi\kappa\vec{\mathcal{N}} + (\nabla\phi \cdot \vec{\mathcal{T}})\vec{\mathcal{T}} - \nabla\phi. \tag{5}$$

This is precisely the gradient flow corresponding to the minimization of the length functional L_ϕ. Since the tangential component of equation (5) may be dropped (see [13]), this may be simplified to

$$\frac{\partial C}{\partial t} = \phi \kappa \vec{\mathcal{N}} - \nabla \phi. \tag{6}$$

The level set version of this is

$$\frac{\partial \Psi}{\partial t} = \phi \|\nabla \Psi\| \mathrm{div}\left(\frac{\nabla \Psi}{\|\nabla \Psi\|}\right) + \nabla \phi \cdot \nabla \Psi. \tag{7}$$

One expects that this evolution should attract the contour very quickly to the feature which lies at the bottom of the *potential well* described by the gradient flow (7). As in [7, 27], we we may also add a constant inflation term, and so derive a modified model of (2) given by

$$\frac{\partial \Psi}{\partial t} = \phi \|\nabla \Psi\| (\mathrm{div}\left(\frac{\nabla \Psi}{\|\nabla \Psi\|}\right) + \nu) + \nabla \phi \cdot \nabla \Psi. \tag{8}$$

Notice that for ϕ as in (3), $\nabla \phi$ will look like a doublet near an edge. Of course, one may choose other candidates for ϕ in order to pick out other features. The point is that the metric ds_ϕ has the property that it becomes small where ϕ is small and vice versa. Thus at such points lengths decrease and so one needs less "energy" in order to move. Consequently, it seems that such a metric is natural for attracting the deformable contour to an edge when ϕ has the form (3).

We have implemented this snake model based on the algorithms of Osher-Sethian [30, 31, 37, 38, 39] and Malladi *et al.* [27].

5 3-D Active Contour Models

In this section, we will show how the 2D active contour model which we have presented may be easily extended to the 3D case. Here we use the corresponding surface evolution equations, gotten by modifying the Euclidean area by a function which depends on the salient features which we wish to capture. For all the relevant concepts on the differential geometry of surfaces, we refer the reader to [11].

Let $S : [0,1] \times [0,1] \to R^3$ denote a compact embedded surface with (local) coordinates (u, v). Let H denote the mean curvature and $\vec{\mathcal{N}}$ the inward unit normal. We set

$$S_u := \frac{\partial S}{\partial u}, \quad S_v := \frac{\partial S}{\partial v}.$$

Then the infinitesimal area on S is given by

$$dS = (\|S_u\|^2 \|S_v\|^2 - \langle S_u, S_v \rangle^2)^{1/2} du dv.$$

Let $\phi : \Omega \to R$ be a positive differentiable function defined on some open subset of R^3. The function $\phi(x, y, z)$ will play the role of the "stopping" function ϕ given above in our snake model (7, 8).

It is a beautiful classical fact that the gradient flow associated to the area functional for surfaces (i.e., the direction in which area is shrinking most rapidly) is given by

$$\frac{\partial S}{\partial t} = H\vec{\mathcal{N}}. \tag{9}$$

(See [45] and the references therein.) What we propose to do is to replace the Euclidean area by a modified area depending on ϕ namely,

$$dS_\phi := \phi dS.$$

For a family of surfaces (with parameter t), consider the ϕ-area functional

$$A_\phi(t) := \int\int_S dS_\phi.$$

Once again, an integration by parts argument gives that

$$\frac{dA_\phi}{dt} = -\int\int_S \langle \frac{\partial S}{\partial t}, \phi H\vec{\mathcal{N}} - \nabla\phi + \text{tangential components}\rangle dS,$$

which after dropping the tangential part becomes

$$\frac{\partial S}{\partial t} = \phi H\vec{\mathcal{N}} - \nabla\phi. \tag{10}$$

The level set version of (10) is given in terms of $\Psi(x, y, z, t)$ by

$$\Psi_t = \phi\|\nabla\Psi\|\text{div}(\frac{\nabla\Psi}{\|\nabla\Psi\|}) + \nabla\phi \cdot \nabla\Psi. \tag{11}$$

As before one may add a constant inflation term to the mean curvature to derive the model

$$\Psi_t = \phi\|\nabla\Psi\|(\text{div}(\frac{\nabla\Psi}{\|\nabla\Psi\|}) + \nu) + \nabla\phi \cdot \nabla\Psi. \tag{12}$$

In the context of image processing, the term ϕ depends on the given 3-D image and is exactly analogous to the stopping term in (7, 8). It is important to note that there is a very big difference between the 2-D and 3-D models discussed here. Indeed, the geometric heat equation will shrink a simple closed curve to a round point without developing singularities, even if the initial curve is *nonconvex*. The geometric model (2) is based on this flow. For surfaces, it is well-known that singularities may develop in the mean curvature flow (9) non-convex smooth surfaces. (The classical example is the dumbbell.) We should note however

that the mean curvature flow does indeed shrink smooth compact convex surfaces to round "spherical" points; see [18].

We should add that because of these problems, several researchers have proposed replacing mean curvature flow by flows which depend on the Gaussian curvature κ. Indeed, define

$$\kappa_+ := \max\{\kappa, 0\}.$$

Then Caselles and Sbert [8] have shown that the *affine invariant flow*

$$\frac{\partial S}{\partial t} = \text{sign}(H)\kappa_+^{1/4}\vec{\mathcal{N}} \tag{13}$$

will (smoothly) shrink rotationally symmetric compact surfaces to ellipsoidal shaped points. Thus one could replace the mean curvature part by $\text{sign}(H)\kappa_+^{1/4}$ in (12). Another possibility would be to use $\kappa_+^{1/2}$ as has been proposed in [28]. See also [42]. (Note that Chow [9] has shown that convex surfaces flowing under $\kappa^{1/2}$ shrink to spherical points.) All these possible evolutions for 3-D contours are now being explored.

6 Applications to Medical Imagery

We will now apply the active contour model derived above to some medical imagery. The implementations we have used are based on the level set evolution methods developed by Osher-Sethian [30, 31, 37, 38, 39], and the techniques in [27]. The equations described in this paper have been coded for the case of active contours on two-dimensional images.

6.1 Numerical Aspects of Level Set Evolution

For 2D active contours, the evolution equation as derived in Section 4 is equation (8),

$$\frac{\partial \Psi}{\partial t} = \phi\|\nabla\Psi\|(\text{div}\left(\frac{\nabla\Psi}{\|\nabla\Psi\|}\right) + \nu) + \nabla\phi\cdot\nabla\Psi,$$

where ν is a constant inflation force and $\kappa := \text{div}(\frac{\nabla\Psi}{\|\nabla\Psi\|})$ is the curvature of the level sets of $\Psi(x, y, t)$. This equation describes a propagating front, and we are interested in its propagation in the plane of an image. It is known that a propagating front may not remain smooth at all times (for example, it may cross itself). For evolution beyond the discontinuities the solutions are required to satisfy an entropy condition to ensure that the front remains physically meaningful at all times. The discrete approximations to the spatial derivatives are thus derived from the entropy condition. Osher-Sethian [31] have given such entropy satisfying

schemes and these have been used successfully in shape modelling [27]. As in[27], we can regard a decomposition of our speed function as,

$$F(\kappa) = \nu + \text{div}\left(\frac{\nabla\Psi}{\|\nabla\Psi\|}\right) = \nu + \kappa, \tag{14}$$

where ν is regarded as the constant passive advection term and the curvature κ is the diffusive term of the speed function. The inflation part in equation (8), i.e., $\nu\phi\|\nabla\Psi\|$ is approximated using upwind schemes. The diffusive part, i.e., $\kappa\phi\|\nabla\Psi\|$ is approximated using usual central differences.

There are also stability implications of the choice of the step sizes, and in [27] it is noted that for the evolution equation used in that work the requirement is $\Delta t = O(\Delta x^2)$. Therefore if small spatial step sizes are used, it forces a small time step and the resulting evolution can be very slow. One way to speed up the evolution is to use a larger inflationary force and move the front faster (recall the advection term causes a constant contraction/expansion of the front). However, in our experience with using the approach in [27] this results in large motion of the front causing "overshooting" of the edge of the feature of interest in the image, because ϕ might not be rigorously zero on the desired contour. This problem is resolved by the evolution in equation (8). $\nabla\phi$ has a behavior similar to a doublet near an edge. Thus, it exerts a "stronger" stopping effect and arrests the evolution of the contour close to an edge. In our experiments we have observed that this arresting behavior of the $\nabla\phi\cdot\nabla\Psi$ term allows use of large inflationary forces, resulting in features being extracted in relatively fewer time steps.

6.2 Contour Extraction Results

We now describe a number of 2D images from which we extracted the contours using the snake/bubble technique which we have previously described. In Figure 1, using an initial bubble, we find the boundary of the left ventricle in an MRI heart image. In Figure 2, the snake (inward) evolution is utilized for the same purpose in another MRI image. Figure 3, illusrates bubbles capturing the edge of a cyst in a breast ultrasound image. Finally, in Figure 4, we indicate the finding of a complicated contour in an MRI brain image again using expanding bubbles.

7 Conclusions

In this paper, we have applied the novel active contour model formulated in [20, 21] to a number of medical images. The power of this technique in extracting features from even rather noisy medical images has been demonstrated. Our approach is geometric based on image-dependent Riemannian metrics and the associated gradient flows for active contour

models. We are now working on fast, reliable implementations of the 3D mean curvature equations for the volumetric segmentation of medical images.

References

[1] L. Alvarez, F. Guichard, P. L. Lions, and J. M. Morel, "Axiomes et equations fondamentales du traitement d'images," *C. R. Acad. Sci. Paris*, 315:135–138, 1992.

[2] L. Alvarez, F. Guichard, P. L. Lions, and J. M. Morel, "Axioms and fundamental equations of image processing," Report #9216, CEREMADE, Université Paris Dauphine, 1992.

[3] L. Alvarez, F. Guichard, P. L. Lions, and J. M. Morel, "Axiomatisation et nouveaux operateurs de la morphologie mathematique," *C. R. Acad. Sci. Paris* 315:265–268, 1992.

[4] L. Alvarez, P. L. Lions, and J. M. Morel, "Image selective smoothing and edge detection by nonlinear diffusion," *SIAM J. Numer. Anal.* **29**, pp. 845-866, 1992.

[5] L. Alvarez and J. M. Morel, "Formalization and computational aspects of image analysis," Report #0493, Department of Information and Systems, Universidad de las Palmas de Gran Canaria, 1993.

[6] A. Blake and A. Yuille, *Active Vision*, MIT Press, Cambridge, Mass., 1992.

[7] V. Caselles, F. Catte, T. Coll, and F. Dibos, "A geometric model for active contours in image processing," Technical Report #9210, CEREMADE, Université Paris Dauphine, 1992.

[8] V. Caselles and C. Sbert, "What is the best causal scale-space for 3D images?," Technical Report, Department of Math. and Comp. Sciences, University of Illes Balears, 07071 Palma de Mallorca, Spain, March 1994.

[9] B. Chow, "Deforming convex hypersurfaces by the nth root of the Gaussian curvature," *J. Differential Geometry* **22**, pp. 117-138, 1985.

[10] L. D. Cohen, "On active contour models and balloons," *CVGIP: Image Understanding* **53**, pp. 211-218, 1991.

[11] M. P. Do Carmo, *Differential Geometry of Curves and Surfaces*, Prentice-Hall, Inc., New Jersey, 1976.

[12] M. P. Do Carmo, *Riemannian Geometry*, Prentice-Hall, Inc. New Jersey, 1992.

[13] C. L. Epstein and M. Gage, "The curve shortening flow," in *Wave Motion: Theory, Modeling, and Computation*, A. Chorin and A. Majda, Editors, Springer-Verlag, New York, 1987.

[14] M. Gage and R. S. Hamilton, "The heat equation shrinking convex plane curves," *J. Differential Geometry* **23**, pp. 69-96, 1986.

[15] I. M. Gelfand and S. V. Fomin, *Calculus of Variations*, Prentice-Hall, Englewood Cliffs, N. J., 1963.

[16] M. Grayson, "The heat equation shrinks embedded plane curves to round points," *J. Differential Geometry* **26**, pp. 285-314, 1987.

[17] A. Gupta, L. von Kurowski, A. Singh, D. Geiger, C. Liang, M. Chiu, P. Adler, M. Haacke, and D. Wilson, "Cardiac MRI analysis: segmentation of myocardial boundaries using deformable models," Technical Report, Siemens Corporate Research, Princeton, NJ, 1995.

[18] G. Huisken, "Flow by mean curvature of convex surfaces into spheres," *J. Differential Geometry* **20**, pp. 237-266, 1984.

[19] M. Kass, A. Witkin, and D. Terzopoulos, "Snakes: active contour models," '*Int. Journal of Computer Vision* **1**, pp. 321-331. 1987.

[20] S. Kichenassamy, A. Kumar, P. Olver, A. Tannenbaum, and A. Yezzi, "Gradient flows and geometric active contours," *Proc. ICCV*, June 1995. September 1994.

[21] S. Kichenassamy, A. Kumar, P. Olver, A. Tannenbaum, and A. Yezzi, "Conformal curvature flows: from phase transitions to active vision," to appear in *Archives of Rational Mechanics and Analysis.*

[22] B. B. Kimia, A. Tannenbaum, and S. W. Zucker, "Toward a computational theory of shape: An overview", *Lecture Notes in Computer Science* **427**, pp. 402-407, Springer-Verlag, New York, 1990.

[23] B. B. Kimia, A. Tannenbaum, and S. W. Zucker, "Shapes, shocks, and deformations, I," *Int. J. Computer Vision*, 1995.

[24] B. B. Kimia, A. Tannenbaum, and S. W. Zucker, "On the evolution of curves via a function of curvature, I: the classical case," *J. of Math. Analysis and Applications* **163**, pp. 438-458, 1992.

[25] R. J. LeVeque, *Numerical Methods for Conservation Laws*, Birkhäuser, Boston, 1992.

[26] P. L. Lions, *Generalized Solutions of Hamilton-Jacobi Equations*, Pitman Publishing, Boston, 1982.

[27] R. Malladi, J. Sethian, and B. Vemuri, *Shape modeling with front propagation: a level set approach, IEEE Trans. Pattern Anal. Machine Intell.* **17**, pp. 158-175, 1995.

[28] P. Neskovic and B. Kimia, "Three-dimensional shape representation from curvature-dependent deformations," Technical Report #128, LEMS, Brown University, 1994.

[29] P. Olver, G. Sapiro, and A. Tannenbaum, "Geometric invariant evolution of surfaces and volumetric smoothing," submitted for publication in *SIAM J. Math. Anal.*, 1994.

[30] S. Osher, "Riemann solvers, the entropy condition, and difference approximations," *SIAM J. Numer. Anal.* **21**, pp. 217-235, 1984.

[31] S. J. Osher and J. A. Sethian, "Fronts propagation with curvature dependent speed: Algorithms based on Hamilton-Jacobi formulations," *Journal of Computational Physics* **79**, pp. 12-49, 1988.

[32] S. Osher and L. I. Rudin, "Feature-oriented image enhancement using shock filters," *SIAM J. Numer. Anal.* **27**, pp. 919-940, 1990.

[33] P. Perona and J. Malik, "Scale-space and edge detection using anisotropic diffusion," *IEEE Trans. Pattern Anal. Machine Intell.* **12**, pp. 629-639, 1990.

[34] M. H. Protter and H. F. Weinberger, *Maximum Principles in Differential Equations,* Springer-Verlag, New York, 1984.

[35] S. Raganath, "Contour extraction from cardiac MRI studies using snakes," *IEEE Trans. on Medical Imaging* **14**, pp. 328-338, 1995.

[36] G. Sapiro and A. Tannenbaum, "On invariant curve evolution and image analysis," *Indiana Univ. Journal of Math.* **42**, 1993.

[37] J. A. Sethian, *An Analysis of Flame Propagation*, Ph. D. Dissertation, University of California, 1982.

[38] J. A. Sethian, "Curvature and the evolution of fronts," *Commun. Math. Phys.* **101**, pp. 487-499, 1985

[39] J. A. Sethian, "A review of recent numerical algorithms for hypersurfaces moving with curvature dependent speed," *J. Differential Geometry* **31**, pp. 131-161, 1989.

[40] J. A. Sethian and J. Strain, "Crystal growth and dendritic solidification," *Journal of Computational Physics* **98**, 1992.

[41] M. Spivak, *A Comprehensive Introduction to Differential Geometry*, Publish or Perish Inc, Berkeley, California, 1979.

[42] H. Tek and B. Kimia, "Deformable bubbles in the reaction-diffusion space," Technical Report #138, LEMS, Brown University, 1994.

[43] D. Terzopoulos and R. Szelski, "Tracking with Kalman snakes," in *Active Vision* edited by A. Blake and A. Zisserman, MIT Press, Cambridge, Mass., 1992.

[44] D. Terzopoulos and A. Witkin, "Constraints on deformable models: recovering shape and non-rigid motion," Artificial Intelligence **36**, pp. 91-123, 1988.

[45] B. White, "Some recent developments in differential geometry," *Mathematical Intelligencer* **11**, pp. 41-47, 1989.

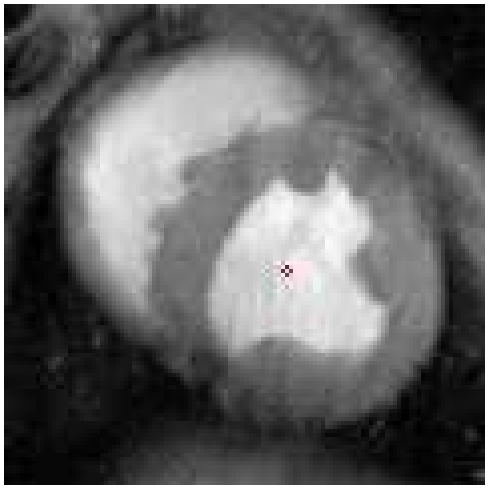

(a)

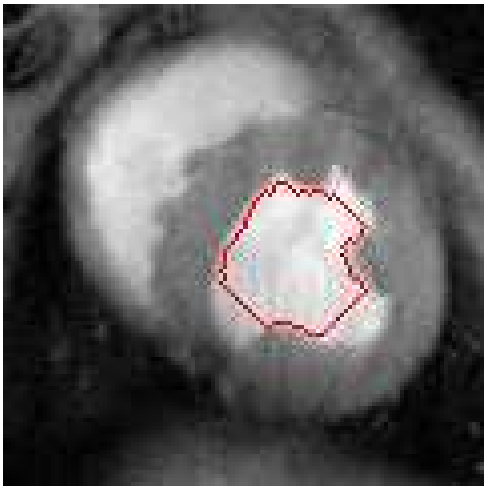

(b)

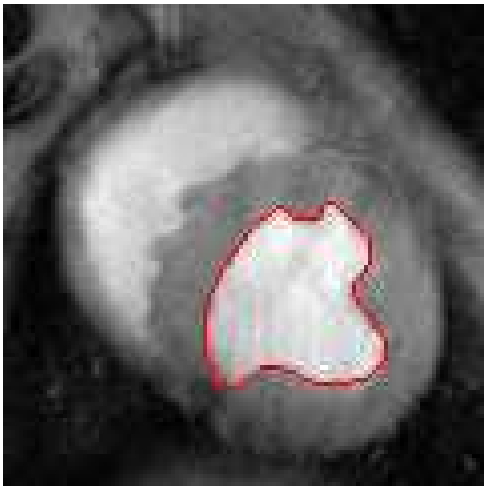

(c)

Figure 1: Contour extraction from MRI heart image via bubble

(a)

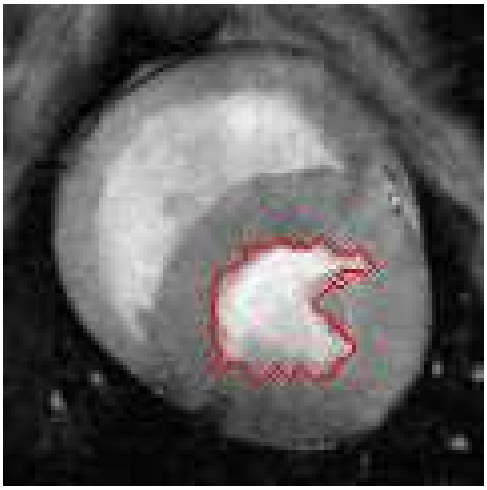

(b)

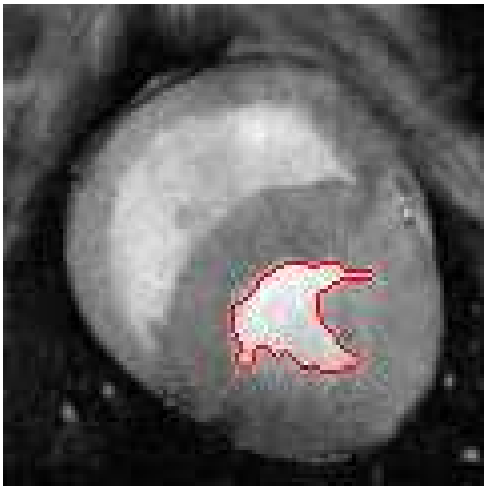

(c)

Figure 2: Contour extraction from MRI heart image via snake

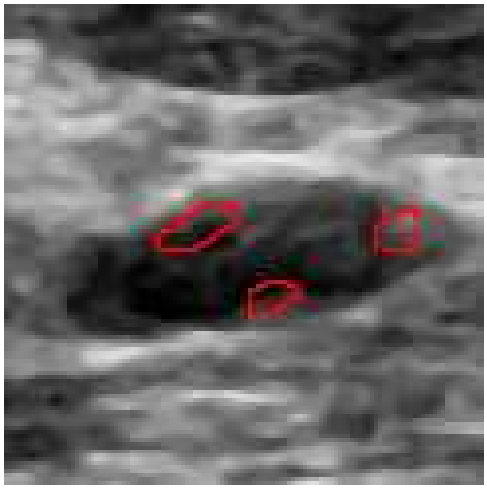

(a)

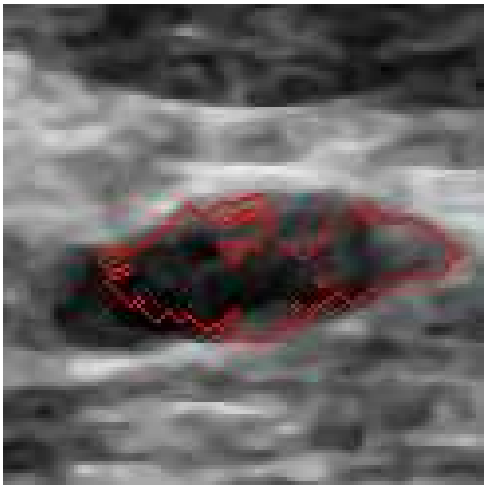

(b)

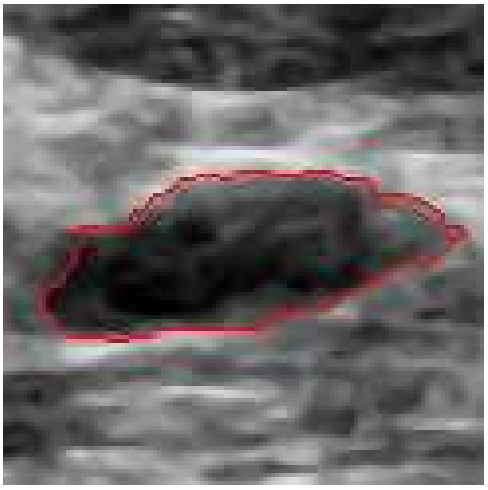

(c)

Figure 3: Contour extraction of cyst from ultrasound breast image via bubbles

(a)

(b)

(c)

Figure 4: Contour extraction from MRI brain image via bubble